HEAT TRANSFER MODELING OF LOCAL THERMAL EXCITATION FOR SURFACE CRACK DETECTION AND CHARACTERIZATION

G. N. Kervalishvili, J. Schlichting, Ch. Maierhofer, M. Kreutzbruck
BAM Federal Institute for Materials Research and Testing, Berlin, Germany

1. Introduction

Open surface cracks are common damage patterns in structures that are subject to cyclic stresses in normal service. These cracks will inevitably grow and potentially lead to in-service failure. For example in low ductility, high performance steel constructions, these cracks not only affect steel durability, but also reduce the strength and impermeability. From the sustainability viewpoint of civil infrastructures, the early non-destructive diagnostic and quantification of open surface defects would allow pertinent preventive maintenance without having to dismount and prematurely change robust components.

Active infrared thermography [1] has also become a powerful tool among other non-destructive diagnostic [2, 3] methods. Nowadays, the infrared (IR) thermal imaging technique is widely used for the non-contact inspection of materials by visualizing thermal surface contrasts after a thermal excitation by flash or halogen lamps [4], and/or IR heaters [5]. Also, using thermography methods for non contact surface temperature observation experiences a growing interest in the laser material interaction field (see, for example Refs. [6-8]). Therefore, modelling of the thermal phenomena which occur during and after laser treatment of solids is necessary. This kind of heat transfer simulations are usually connected to industrial applications and developing of the new research activities requires new simulation models for laser-solid interactions. The 2D and 3D numerical calculation is usually done for the interactions, where the laser changes the material or/and material surface properties, such as laser welding [9, 10], or surface treatment processes [11, 12]. On the other hand, research activity, where a laser beam is used as a local excitation mechanism for solids in thermography investigation [13-15], is actively developing. For example in Ref. [13], a technique to measure thermal diffusivity using laser excited thermography is described, together with the 2D axisymmetric model of the heat transfer, which leads to the identification of diffusivity of thermal barrier coatings. The experimental results that have been obtained using laser beam heating and which have been compared with a 2D numerical model are presented in Ref. [15]. In the given model, a selected part of the surface was kept at a constant elevated temperature, i.e. the laser beam was modelled as a constant temperature boundary condition and not as a heat flux boundary condition. In order to use the laser excited thermography technique with maximum efficiency, the developing of new simulation models is essential. In Ref. [16] an advanced technique to characterize the crack depth by active thermography is presented, where for local excitation mechanism a Nd:YAG laser beam was used.

In the presented work the heat transfer process induced by the local thermal excitation (Nd:YAG laser beam) for surface crack detection and characterization is simulated using a commercial finite element (FEM) analysis and solver software package [17]. The 2D and 3D heat transfer process in solid specimens is calculated for the surface cracks with known geometry (width and depth in 2D cases, and length in 3D cases) and thermal properties. Simulations for 2D cases have been done for fixed width and depth of cracks, where the optimal positions for reference points and heat flux have been investigated. Then these simulations with given heating/detection parameters have been repeated for 3D cases, where the influence of crack length on the lateral heat flow has been studied. For post-processing and data visualization commercial software [17, 18] is used. In contrast to the previous works full 3D numerical simulations of heat transfer are done. Furthermore, the laser spot is modelled as a heat flux boundary condition. Also, the radiation and convection boundary conditions and air heat conduction inside the cracks are taken into account. Comparison of 2D and 3D simulation results is showing that 2D modelling is valid only for qualitative estimation of these processes and only the 3D modelling will allow accomplishing a quantitative level of comparison.

2. Model Description

Transient 3D heat transfer equation in solids can be written in the following form:

$$\rho c \frac{\partial T}{\partial t} - \frac{\partial}{\partial x}\left(k_x \frac{\partial T}{\partial x} \right) + \frac{\partial}{\partial y}\left(k_y \frac{\partial T}{\partial y} \right) + \frac{\partial}{\partial z}\left(k_z \frac{\partial T}{\partial z} \right) = Q\,. \qquad (1)$$

Here, ρ is the density, c is the specific heat capacity, T is absolute temperature, t is time, k is thermal conductivity, and Q is a heat source/sink (in our cases it is zero). The Nd:YAG laser power was taken into account as a surface heat flux, which acts only on a fixed $S_0 = \pi r_0^2$ surface area, where $r_0 = 0.5\,\text{mm}$ is the laser beam radius. The heat distribution of the laser beam had the following form:

$$q_0(t) = const \cdot \left(P_L / S_0\right) \cdot \left(H(t - t_1) - H(t - t_2)\right), \qquad (2)$$

where $H(t)$ is the Heaviside step function, which describes the fact, that the laser heats the specimen surface only for the given $\Delta t = t_2 - t_1$ time interval (here, $t_1 = 0$ and $t_2 = 2\,\text{s}$ is used); P_L is a laser power (in our cases equal to 2 W), and *const* is a constant coefficient equal to 0.8, which in combination with P_L represents the amount of the heat flux absorbed by the surface.

In order to study the influences of heat conduction, convection and radiation (surface to surface and surface to ambient) on the lateral heat flow through the crack, simulations have been done for two cases: in vacuum and in air. Therefore, different boundary conditions were used in each case. The generalized boundary condition for heat flux can be written in the following form:

$$n \cdot \left(k \nabla T\right) = q_0 + h\left(T_{\text{inf}} - T\right) + \sigma \varepsilon \left(T_{amb}^4 - T^4\right). \qquad (3)$$

Here, ε is emissivity, σ is Stefan–Boltzmann constant, q_0 is the term which describes the Nd:YAG laser heat flux (Eq. (2)), and h is a constant convective heat transfer coefficient. In

Eq. (3) second and third terms are accounting for the convection and radiation heat fluxes, respectively. In the case of surface to surface radiation, for crack boundaries, the following equation applies:

$$n \cdot (k \nabla T) = \varepsilon \left(G - \sigma T^4 \right), \tag{4}$$

where G is irradiation ($G = \sigma T_{amb}^4$ in the surface to ambient radiation case), more details can be found in Ref. [19]. If $q_0 = 0$ and all coefficients are set to zero then Eq. (3) turns in an insulation boundary condition:

$$n \cdot (k \nabla T) = 0 . \tag{5}$$

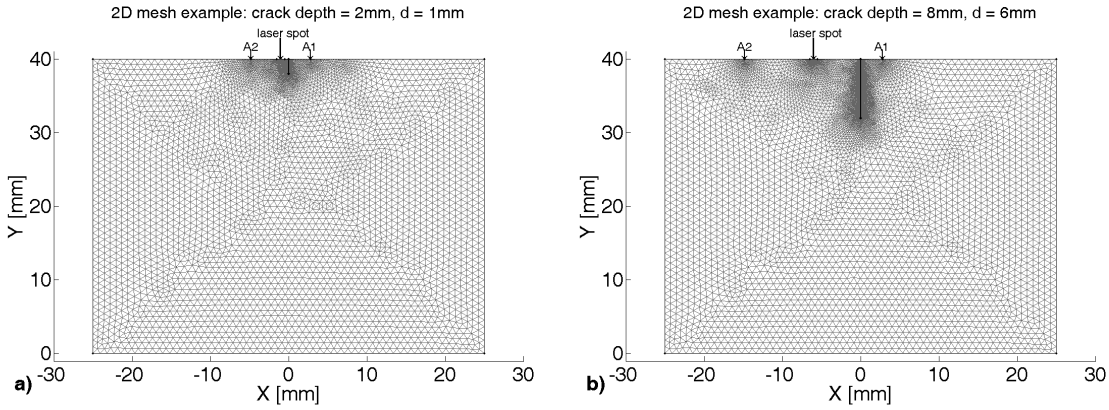

Figure 1. 2D Mesh examples for fixed value of crack width 0.1 mm and crack depths: a) 2 mm, b) 8 mm. The specimen has the following geometrical sizes: height 40 mm, width 50 mm. Definition of *A1* and *A2* is given in Fig. 3.

The commercial software [17] used here for simulations controls the time step values automatically (initial time step was about 10^{-5}s to 10^{-4}s for both 2D and 3D cases). The number of mesh elements was about 15,000 to 21,000 for 2D cases and about 500,000 to 900,000 for 3D ones, depending on the crack size. For higher accuracy of the numerical results it was necessary to decrease the grid size at heat flux and crack boundaries, and at reference point regions. The mesh examples for 2D and 3D cases are shown in Fig. 1 and in Fig. 2, respectively.

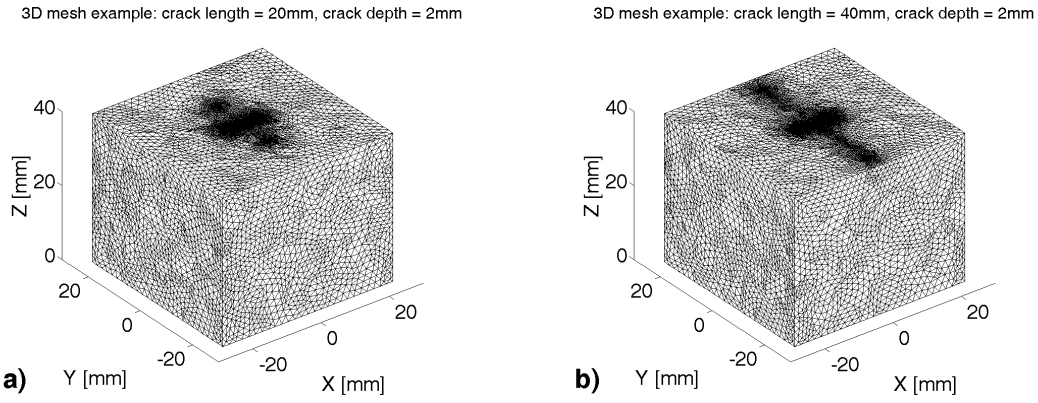

Figure 2. 3D Mesh examples for fixed values of crack width 0.1 mm, crack depth 2 mm and crack lengths: a) 20 mm, b) 40 mm. The specimen has the following geometrical sizes: height 40 mm, width 50 mm, and length 50 mm.

The thermal parameters of st37 construction steel used in presented work are shown in Table 1. The heat transfer simulations have been done for the laser beam power of 2 W. The duration of heating was 2 s and the total simulated time was 6 s including the heating time. Simulations have been done for different crack depths in 2D and for different crack depths and lengths in 3D. For all simulated cases the different boundary conditions inside the cracks were applied. Also, different material properties of the crack, i.e. vacuum and air, were taken into account. This gives us possibility to investigate the influence of heat conduction, radiation (surface to surface and surface to ambient) and convection on the lateral heat flow through the crack. The geometrical parameters of the cracks used in the simulations are also shown in Table 1. Additionally, the influence of the distance between the laser spot and crack position *d* was taken into account, i.e. each model with fixed values of crack depth in 2D was simulated for different distance values.

Table 1. Simulation parameters

Thermal parameters of st37	k = 56.7 W m^{-1}K^{-1}	c = 470 J kg^{-1}K^{-1}	ρ = 7841 kg m^{-3}	
Geometrical sizes of the specimen in mm	width = 50, height = 40; length = 50 (3D cases)			
Laser beam power P_L in W	2.0			
Crack width in mm	0.1			
Crack depth in mm	2.0	4.0	6.0	8.0
Crack length in mm (3D cases)	5.0	10.0	20.0	40.0
Distance between laser spot and crack *d* in mm	1.0	2.0	3.0	6.0
Distance between laser spot and reference point *e* (Fig. 2) in mm	3.8	4.8	5.8	8.8

3. Results

The lateral heat transfer, affected by crack position and size, allows us to detect the temperature differences between two reference points located at the different sides of the crack. These two reference points defined as *A1* and *A2* (laser spot location side), are in equal distance from the laser spot (Fig. 3). The distances between reference points and laser spot are equal. This distance *e* is increasing, when the distance between laser spot and crack *d* increases $e = c + d$, where *c* is fixed and equal to 2.8 mm.

The simulations in 2D and 3D have been done for different boundary conditions. The influence of the radiation boundary condition on the conduction heat flow in both cases (vacuum or air material properties of the crack) was negligible. The influence of convective heat flow on the conductive one through the crack in the case of air was also negligible, i.e. the influence of the both effects on the simulation results was less than 0.1%.

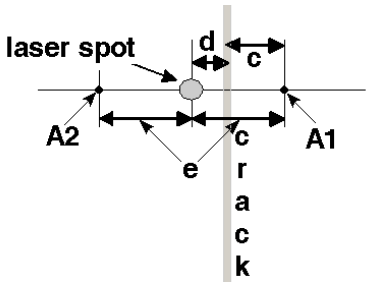

Figure 3. Two reference points *A1* and *A2* are located in equal distance to the laser spot, where *c* is fixed and equal to 2.8 mm. The values of *d* are given in Table 1.

3.1 Results for 2D Geometries

2D simulations have been done for fixed values of crack width 0.1 mm and for four different values of the crack depth: 2, 4, 6 and 8 mm, respectively (Table 1). The distance between laser spot and crack *d* had the following values: 1, 2, 3, and 6 mm. The temperature distributions for a crack depth of 8 mm, and for a distance *d* of 1 mm and 6 mm are shown in Fig. 4. On these figures simulation results are shown for the time point at which the heat flux is switched off ($t = 2$ s). The temperature differences between reference points *A2* and *A1* at four different laser spot locations relative to crack position for the crack depths of 2 mm, 4 mm, 6 mm and 8 mm are plotted in Fig. 5. Please note that the reference points positions depend on the distance between laser spot and crack, and change linearly with this distance (Table 1). As we can see the temperature differences are higher for the laser spot locations closer to the crack position. Therefore, for the best identification and characterization of surface defects the closest possible position of heat source from a crack is desirable. From the given plots one can see that an increase of the crack depth leads to an increase of the temperature differences between reference points *A2* and *A1* (Fig. 5).

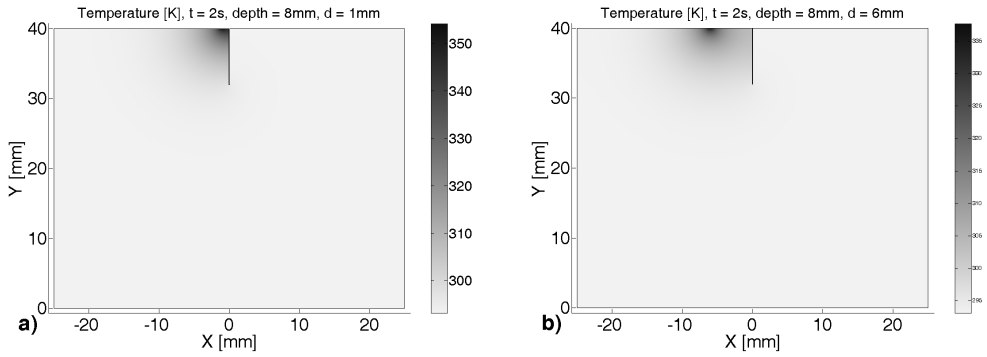

Figure 4. Temperature distribution for fixed values of crack width 0.1 mm, crack depth 2 mm and for different heat source positions: a) *d* = 1 mm, b) *d* = 6 mm.

The same holds for the case, when crack is filled by air, i.e. conductive heat transfer through the crack is taken into account. In Fig. 6a the temperature difference between the reference points is plotted as a function of crack depth for fixed crack width of 0.1 mm and for the distance *d* equal to 1 mm. In Fig. 6b, for the same crack parameters as before, the difference between heat transfer in

vacuum (no heat transfer trough the crack) and conductive heat transfer in air is shown as a function of crack depth. One can see that these differences are very small (about 3%) and therefore, the temperature difference between reference points *A2* and *A1* is defined mainly by the heat conduction in steel.

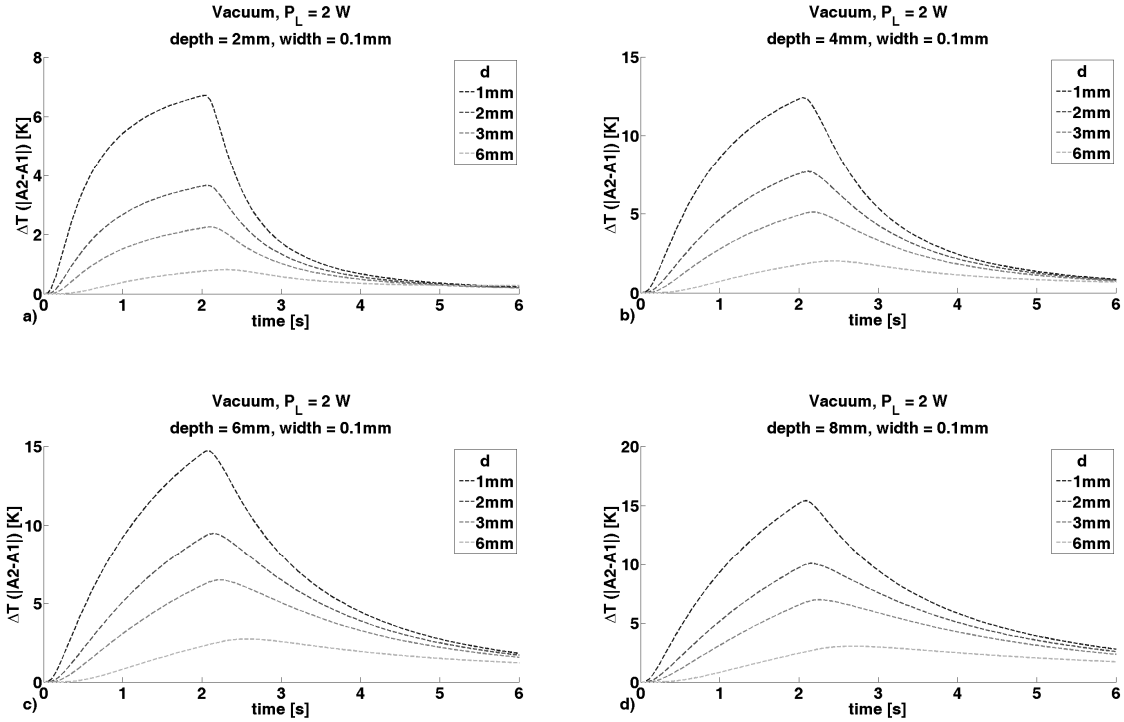

Figure 5. Temperature difference between reference points *A2* and *A1* as a function of time and distance *d* between laser spot and crack positions, for four different crack depths: a) 2 mm, b) 4 mm, c) 6 mm, d) 8 mm.

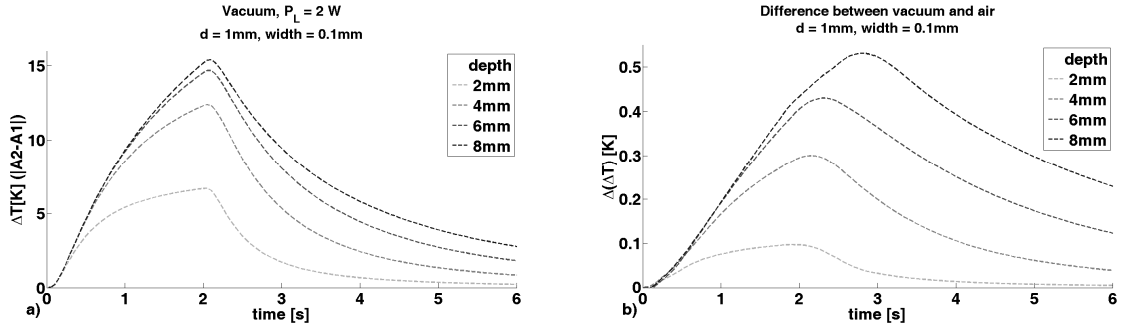

Figure 6. Temperature difference between reference points *A2* and *A1* as a function of time and crack depth, for fixed values of *d* and crack width, 1 mm and 0.1 mm, respectively. The plots are done for two different conditions: a) vacuum, b) difference between vacuum and air.

3.2 Results for 3D Geometries

3D simulations have been done for fixed values of crack width and distance between laser spot and crack, 0.1 mm and 1 mm, respectively. For the given simulations, length and depth of crack have been varied (see Table 1). The crack length and depth had the following values: 5, 10, 20, 40 mm

and 2, 4, 6, 8 mm, respectively. Isosurface plots of the temperature distribution for a crack depth of 8 mm are shown in Fig. 7. On these figures the top surface temperature distribution are shown for

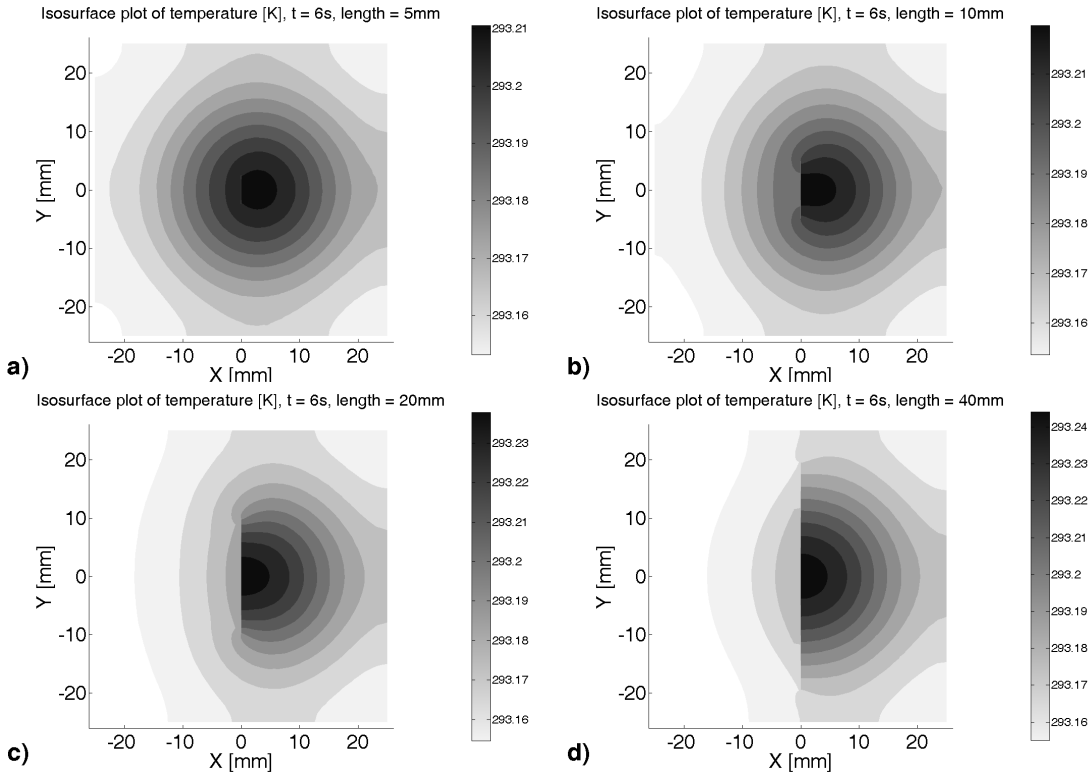

Figure 7. Isosurface plots of the temperature distribution for the fixed values of crack width and depth, 0.1 mm and 8 mm, respectively, and for crack lengths: a) 5 mm, b) 10 mm, c) 20 mm, d) 40 mm. Time is equal to 6s.

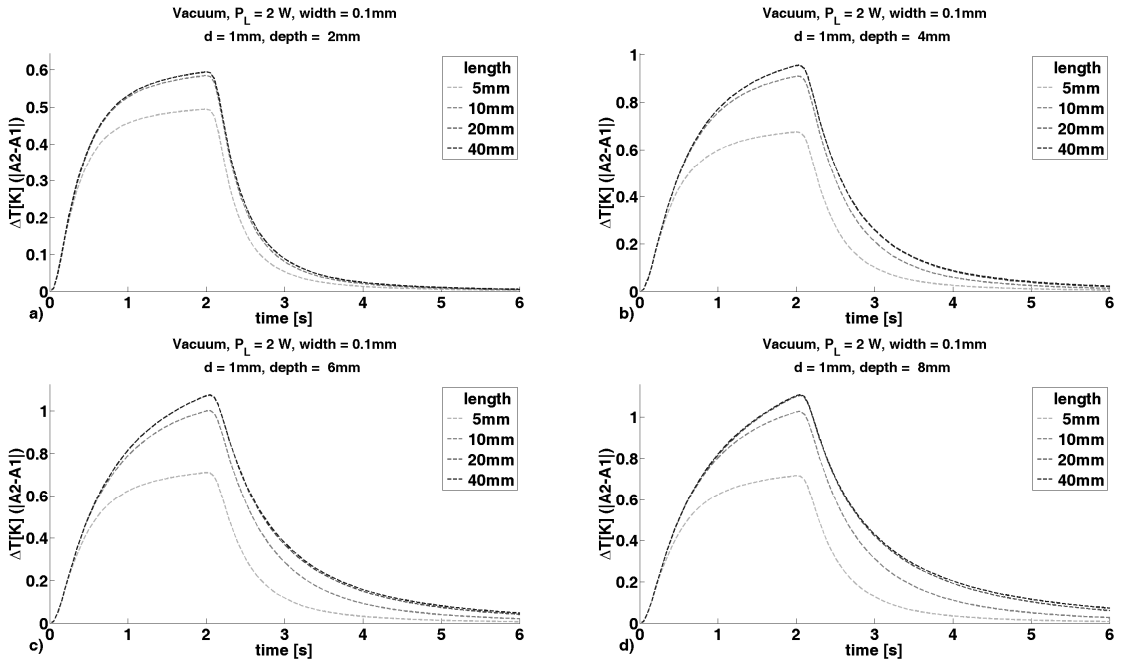

Figure 8. Temperature difference between reference points *A2* and *A1* as a function of time and crack length, for four different crack depths: a) 2 mm, b) 4 mm, c) 6 mm, d) 8 mm.

the simulation end time point ($t = 6\,\mathrm{s}$). As we can see from the given plots the temperature distribution for cracks with large length scales looks more like a 2D one. While, for the cracks with small length scales the temperature distribution is effected by the lateral heat flow (means of crack length). The temperature differences at the reference points for the 3D cases for a crack width of 0.1 mm and for a distance *d* of 1 mm are shown in Fig. 8. These temperature differences are shown as a function of time and crack length for the following fixed value of crack depths: 2 mm (Fig. 8a), 4 mm (Fig. 8b), 6 mm (Fig. 8c), and 8 mm (Fig. 8d). As we can see an increase of the crack depth leads to an increase of the temperature differences between reference points. Also, one can see from Fig. 8a the temperature differences even in the case of relatively small crack sizes are large enough for crack detection and characterization. For the values of crack length more then 10 mm the temperature differences do not changes much, but still allow characterizing cracks with depth values less then 6 mm (Fig. 9b-d). Overall, one can conclude that for the given simulated 3D cases the temperature differences are large enough for crack detection and characterization, even for such small value of laser power as 2 W.

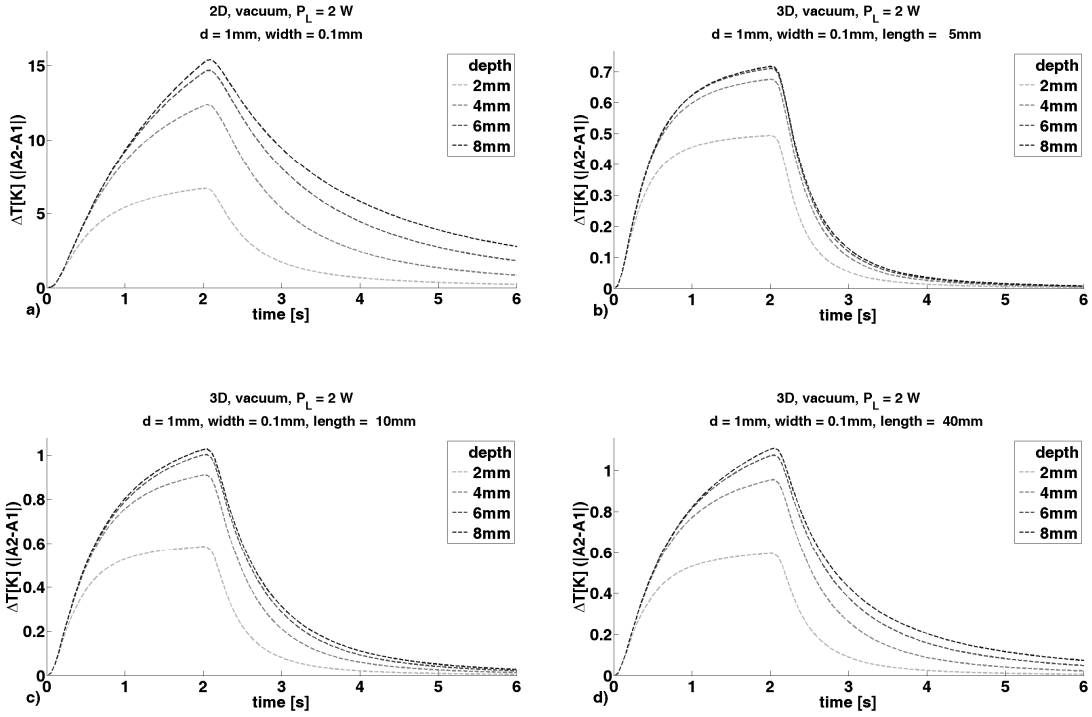

Figure 9. Temperature difference between reference points *A2* and *A1* as a function of time and crack depth, for 2D case (a) and for three different crack lengths in 3D: b) 5 mm, c) 10 mm, d) 40 mm.

3.3 Comparison between 2D and 3D Results

The temperature differences at the reference points, for 2D and 3D cases, as a function of time are shown in Fig. 9. As one can see from the given plots, the maximum values of temperature differences between reference points *A2* and *A1* are several times larger in 2D cases (Fig. 9a) in contrast to the 3D ones (Fig.9b-d). It seems that for these kinds of processes, where circular heat

sources are used as local excitation mechanisms, 2D modelling allows only qualitative descriptions. For the quantitative characterizations full 3D modelling is essential, because there are at least one order of magnitude differences between 2D and 3D simulation results (Fig.9).

4. Summary

In the presented paper the use of local excitation (laser beam) for crack detection and characterization is simulated. As we could see, using the temperature differences between two reference points was large enough to detect and characterize the crack, even for such small value of laser power as 2 W. The influence of radiation and convection on the temperature difference was negligible (about 0.1%). The influence of heat conduction, in case of crack with air, was very small (about 3%). The main mechanism which influences the temperature differences between the reference points is the heat conduction in steel. From the presented results one can see that temperature differences are increasing with an increase of the crack depth or the crack length. Better resolution and characterization of the crack depths and lengths should be achieved with increased duration of heating time or the laser power. We could also see that the best position for the laser spot to characterize the crack is the closest one. Also, comparison of 2D and 3D simulation results for circular heat source used as local excitation mechanism had showed that only full 3D modelling will allow accomplishing a quantitative level of comparison between experimental and simulation results.

References

[1] X. Maldague. Theory and Practice of Infrared Technology for Non Destructive Testing, Wiley, New York, 2001.

[2] M. J. Golis. An Introduction to Nondestructive Testing, American Society of Nondestructive Testing, Columbus, OH, 1991.

[3] L. Cartz. Nondestructive Testing, ASM International, Materials Park, Ohio, (1995).

[4] X. Maldague, S. Marinetti. Pulse phase infrared thermography, Journal of Applied Physics, vol. 79, pp. 2694-2698, 1996.

[5] Ch. Maierhofer, M. Rollig, R. Arndt, M. Kreutzbruck. Influence of Surface Properties on the Detection and Quantification of Voids in Concrete Structures Using Active Thermography, AIP Conf. Proc. 1096, pp. 1505-1511, 2009.

[6] A. Al-Habaibeh et al. A novel approach for quality control system using sensor fusion of infrared and visual image processing for laser sealing of food containers, Meas. Sci. Technol. 15, pp. 1995-2000, 2004.

[7] U. Siemer. Simulation and evaluation of new thermographic techniques for the deployment in the automotive industry, in European Federation for Non-Destructive Testing, ECNDT 2006, Berlin, Germany, 2006.

[8] M. Spekaa, S. Matteïa, M. Pilloza, M. Ilie. The infrared thermography control of the laser welding of amorphous polymers, NDT & E International vol. 41, pp. 178-183, 2008.

[9] A. P. Mackwood, R. C. Crafer. Thermal modelling of laser welding and related processes: a literature review, Optics & Laser Technology, vol. 37, pp. 99-115, 2005.
[10] S. Mattei, D. Grevey, A. Mathieu, L. Kirchner. Using infrared thermography in order to compare laser and hybrid (laser+MIG) welding processes, Optics & Laser Technology vol. 41, pp. 665-670, 2009.
[11] Z. Zhao, C. Wang, M. Li, L. Wang. Nd:YAG laser surface treatment of copper to improve the wettability of Sn3.5Ag solder on copper, Surface and Coatings Technology vol. 200, pp. 2181-2186, 2005.
[12] M. Rohde, O. Baldus, D. Dimitrova, S. Schreck. Numerical Simulation of Fast Dynamic Laser-Surface Interaction during Laser-Induced Modification Processes of Ceramic Substrates, International Journal of Thermophysics vol. 26, pp. 1063-1073, 2005.
[13] P.G. Bison, F. Cernuschi, E. Grinzato, S. Marinetti, D. Robba. Ageing evaluation of thermal barrier coatings by thermal diffusivity, Infrared Physics & Technology, vol. 49, pp. 286-291, 2007.
[14] V. Carl, Messtechnik & Prüfsysteme. Webpage: www.t-zfp.de, (http://www.t-zfp.de/Technik/Laser/Finite_Elemente/finite_elemente.html).
[15] A. Rashed, D.P. Almond, D.A.S. Rees, S. Burrows, S. Dixon. Crack Detection by Laser Spot Imaging Thermography, AIP Conf. Proc. 894, pp. 500-506, 2007.
[16] J. Schlichting, G.N. Kervalishvili, Ch. Maierhofer, M. Kreutzbruck. Charakterisierung von Rissen mittels Laser angeregter aktiver Thermografie, Thermografie-Kolloquium 2009 der DGZfP, Stuttgart, Deutschland, 2009.
[17] COMSOL Multiphysics, COMSOL Multiphysics Heat Transfer Module. COMSOL Multiphysics User's Guide. Version: COMSOL Multiphysics 3.5a.
[18] MATLAB, Version: MATLAB R2007b.
[19] F.P. Incropera, D.P. DeWitt. Fundamentals of Heat and Mass Transfer, 4th ed., John Wiley & Sons, 1996.